Nucleic Acid Based Fluorescent Nanothermometers

Sara Ebrahimi,[†,‡] Yousef Akhlaghi,[†] Mohsen Kompany-Zareh,[*,†] and Åsmund Rinnan[‡]

[†]Department of Chemistry, Institute for Advanced Studies in Basic Sciences (IASBS), Zanjan, 45137-66731, Iran and [‡]Department of Food Science, Faculty of Sciences, University of Copenhagen, DK-1958 Frederiksberg, Denmark

ABSTRACT Accurate thermometry at micro- and nanoscales is essential in many nanobiotechnological applications. The nanothermometers introduced in this paper are composed of labeled molecular beacons (MBs) comprising gold nanoparticles (AuNPs) on which, depending on application, many MBs of one or more types are immobilized. In this design, three differently labeled MBs with different thermostabilities function as the sensing elements, and AuNPs act as carriers of the MBs and also quenchers of their fluorophores. This flexible design results in a number of nanothermometers with various temperature-sensing ranges. At the lowest temperature, the MBs are in the closed form, where they are quenched. By increasing the temperature, the MBs start to open with respect to their melting points (T_m), and as a result, the fluorescence emission will increase. The temperature resolution of the nanoprobes over a range of 15−60 °C is less than 0.50 °C, which indicates their high sensitivity. Such a good temperature resolution is a result of the specific design of the unusual less stable MBs and also presence of many MBs on AuNPs. The reproducibility and precision of the probes are also satisfactory. The multiplex MB nanoprobe is suitable for thermal imaging by fluorescence microscopy.

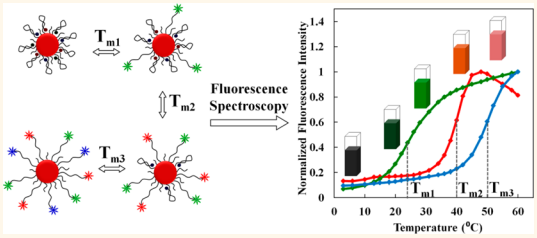

KEYWORDS: nanothermometers · molecular beacons · gold nanoparticles · fluorescence · thermal imaging

As the scale of the most advanced nanobiotechnology research decreases, the requirement for smaller thermometers increases. Accurate thermometry at micro- and nanoscales is still a challenging research topic that is essential in many biotechnological applications and microdevices developed for these purposes.[1,2]

Temperature influences the chemical reactions and equilibria and, as a result, the behavior of biological systems.[3] It is some of the most valuable measurable information from a biochemical system. For example, determination of intracellular temperature has gained attention as an indicator to distinguish between cancer and normal cells.[4] Thus, it is necessary to have a nanodevice that is capable of accurately monitoring temperature and temperature gradients at a submicro scale. Current state-of-the-art noninvasive global temperature measurement techniques, in which the measurement is carried out at a distance, after treating the medium with proper molecular probes (*e.g.*, temperature sensitive fluorophores),[5−8] polymers,[9,10] proteins,[11,12] and nanoparticles (*e.g.*, quantum dots,[13,14] and nanogels[15]), have attracted wide attention. Most of them rely on decreased fluorescence intensities as a result of increased nonradiative decay at higher temperature. There are publications measuring the local temperature of nanoparticles. The temperature profile of the azo-functionalized iron oxide nanoparticle surface when exposed to an alternating magnetic field (AMF) was reported.[16] One type of temperature probe reported in the literature is the nanoparticle−DNA assembly. One example of such a thermometer probe is the dehybridization of double-stranded DNAs bound to gold nanoparticles responding to the radio frequency field.[17] In a recent application, the AMF has been used to local heating of the DNA by functionalized magnetic nanoparticles.[18] The temperature was measured by the extent of dehybridization of the DNA strands with the subsequent release of the fluorophore-labeled strands. The above-mentioned methods were developed to bypass some of the limitations, *e.g.*, difficulty in implementation of invasive methods based on thermocouples and lack of spatial resolution of noncontact methods such as IR thermography.[19,20] Several reviews have

* E-mail: kompanym@iasbs.ac.ir.

Received for review July 7, 2014 and accepted September 29, 2014.

Published online September 29, 2014
10.1021/nn5036944

recently been published to emphasize the importance of designing such nanodevices.[21−24]

An ideal noninvasive fluorescent sensor for nanoscale thermometry should possess several features. The intensity of its signal should be high enough to be distinguished from the background emission. In the case of intracellular application, the sensor must be nontoxic for long-term measurements. In addition, other properties such as measurement of high temperatures with good spatial resolution, rapid response time, and wide temperature sensing range are desirable. For thermal imaging by fluorescence microscopy, in addition to high spatial resolution, a multicolor (multiplex) sensor is beneficial.

Among noninvasive fluorescence thermal sensors, a particularly attractive tool is the molecular beacon (MB).[25] MBs have advantages over conventional probes such as biocompatibility, small size, and their unique temperature-dependent structural features.[26] An MB is a strand of DNA containing a number of bases, dually labeled by a fluorophore and a quencher at its two ends. Its sequence is chosen in such a way that the two ends can hybridize and form a stem-loop structure. The MB is fluorescent in the open form and nonfluorescent in the closed form. Thermal stability of the MBs is mirrored in the melting point, T_m, where half of the MBs are open.[27] The T_m at which the derivative plot of melting curve goes through a maximum is a thermodynamic characteristic of the chosen oligonucleotide sequence. It is worth noting that the T_m of MBs is independent of their concentration.[28] MBs were first used to measure the difference between the temperature given by a macroscopic thermometer stuck onto the microdevices and the true temperature within the corresponding microfluidic chambers.[2,29] Today more sophisticated applications are published, *e.g.*, in thermal mapping.[30] These hairpin-like nucleic acid structures may also be used as temperature sensors in some living organisms.[31]

A shortcoming of the current molecular beacon-based thermometers is that, they rely on only one type of MBs with a limited temperature sensing function. To address this problem and also to utilize multicolor images for thermal imaging, a promising solution is to use a number of MBs with different thermostabilities each labeled with a different pair of fluorophore/quencher.

The choice of quenchers is very important as it can result in a higher quenching efficiency and a lower "off" signal. Although traditional organic quenchers are effective in quenching nearby fluorophores, their quenching efficiencies are usually significantly different from dye to dye.[32,33] For example, DABCYL efficiently quenches the fluorescence of FAM, but it is much less efficient for dyes emitting at longer wavelengths (*e.g.*, Texas red and the cyanine dye Cy5). A different approach is to use gold nanoparticles (AuNPs), well-known ultrahigh fluorescence quenching agents.[34−38] The gold nanoparticles not only function as carriers of many MB structures but also function well as universal quenchers for all of the fluorophores by which the MBs are tagged.

In this study, the proposed AuNP-based thermometers are composed of two or more MBs with different lengths and sequences of duplex stem region, hence, different melting points. Each MB is labeled at one end with a specific fluorophore and attached to the AuNP surface by a thiol linker at the other end. At the lowest temperature, the MB stem-loop structures are all in the closed form. This brings the fluorophores near the AuNP surface where they will be quenched. By increasing the temperature, the stem of the MB structures start to open depending on their melting points. This increases the distance between the fluorophores and the AuNP surface which lead to enhancement of their fluorescence emission. The overall result will be a specific combination of emitted lights at each temperature. The distance between the AuNP surface and the fluorophores when the MBs are in the open form is very critical, because insufficient distance may keep the probe at the quenched state.[39]

Although a number of AuNP-based multiplex nanoassemblies have been developed for detection of DNA, small molecules, and endonucleases,[40−42] no study has reported their application for thermometry, to the best of our knowledge. Here, a critical factor that should be considered is the thermal stability of the MBs. A challenging part of this study was to design a long stem MB with low thermal stability. As will be discussed later, such an "unusual" MB is necessary for the measurement of low temperatures. This is the first application of unusual MBs to construct the thermosensitive nanoassemblies.

Such a nanothermometer is advantageous from different points of view: (1) The presence of dissimilar MBs improves the temperature sensing range of the thermometer. (2) Both multicolor thermal imaging and low temperature resolution measurements can be performed using multiple fluorophores that increase the flexibility of the design. (3) Attachment of many MB probes on each AuNP increases the sensitivity of the nanothermometer. (4) This design does not need different quenchers. (5) The AuNP surface could easily be functionalized for different target specific applications of the nanothermometer.

RESULTS AND DISCUSSION

The basic idea behind the design of multiplex nanothermometer is that, at the lowest temperature, the MBs are all in the closed quenched form. Higher temperatures cause the MBs to start to open with respect to their melting points resulting in an increased fluorescence. The sharpest increase in the fluorescence signal of each MB is expected around its melting point,

which can be obtained from the S-shaped melting curve (the temperature at which the first derivative of the melting curve has the maximum value). The overall result will be a sensitive fluorescence method, which depends on the current temperature of the system, and respond to a wider temperature range than the current single MB-based thermometers.

Designing the Molecular Beacons. The first part of this study is focused on designing the MBs utilizing web-based tools,[43] especially rather unusual less stable ones, as the three temperature sensing units. As the main purpose of this study was to introduce a thermometer for a wide range temperature determination at microscopic scale, three melting points about 22, 38, and 48 °C were chosen as target melting points in the design of the corresponding MBs.

The efficiency of AuNPs to quench the fluorophores is optimal when the distance between them is less than 5 nm. Therefore, it is of importance to design probes in such a manner that the fluorophores are very close to the AuNP in the closed form, and at the same time allowing for a sufficiently long distance between the fluorophore and the AuNP in the open melted form.[39] To do this, the structure of the probes was designed to have rather long stems and large loops and also appending a spacer at the 3′ end of them. As these modifications usually increase the stability of MBs and their T_m, one of the challenging steps of this work was to design long stem MBs with low stability, this is especially critical for the MB probe designed for covering low temperatures ($T_m \sim 22$ °C).

A strategy to theoretically shift the T_m of longer MBs toward lower values is the altering of the stability of the double-helix stem region. By making the double helix less stable, the overall probe would melt at lower temperatures. The stability of a double helix is determined by its free energy; the lower the free energy, the more stable the MB structure. One method to destabilize the MB is using A−T rich stems. Another more effective approach is to insert internal mismatch base pairs (mainly T:T) and also internal loops into the stem region.

To design the desired MB structures, it is also important to find the right sequence of the external loop and the spacer. As thymine has the lowest tendency to be adsorbed on the AuNP surface, it was the preferred nucleotide for these parts.[44] Insertion of internal loops in order to weaken the stem region might cause the MB to fold into completely unwanted secondary structures with quite different melting points; thus, the position of the internal loops should be selected with caution. Using these strategies and by the help of the mfold web server,[43] many potential structures were designed and their optimum secondary structures and corresponding thermodynamic properties under simulated experimental conditions (T_m, assuming a two-state model and minimum free energy) were predicted. We first designed the sequence of a long enough MB without any internal mismatches and loops and then started to reduce the predicted T_m of MB to the desired T_m by changing the GC content of the stem region and also inserting one or several internal mismatch/loops. From the studied sequences, the three best sequences with only one predicted secondary structure were selected to assemble the nanothermometer.

TABLE 1. Oligonucleotides Used in This Study and Their Sequences

name	sequence (5′ → 3′)
OligoF	**FAM**-ATCATAATTATTGTTTTTTTTTTTTTTTACTATTTTTTTGAT-(10T)-$(CH2)_3$-**SH**
OligoTR	**TR**-ATCTAATCATTATTGTTTTTTTTTTTTTTTACTATTATGTTTAGAT-(10T)-$(CH2)_3$-**SH**
OligoA	**ATTO 425**-ATATACATTTGTTTTTTTTTTTTACATATG TATAT-(10T)-$(CH2)_3$-**SH**
OligoT	TTTTTTTTTT-$(CH2)_3$-**SH**
MBTR	**FAM**-ATCTAATCATTATTGTTTTTTTTTTTTTTTACTATTATGTTTAGAT-**Dabcyl**
MBpTR	**FAM** -ATCTAACATATGTTTTTTTTTTTTTTTTACATATGTTAGAT-**Dabcyl**
MBpF	**FAM**-ATCAAAATGTTTTTTTTTTTTTTTTACATTTTGAT-(10T)-$(CH2)_3$-**SH**

Three designed MBs, their proposed structures, and also their melting points can be observed in the Supporting Information (Figure S1). The MB with T_m = 22.4 °C was named oligoF as it was modified with FAM at 5′ end upon synthesis. The MBs with T_m = 38.7 °C, and T_m = 48.7 °C, were modified with Texas red and Atto 425 fluorphores and named oligoTR and oligoA respectively. The oligonucleotide sequences used in this work are listed in Table 1. The conditions under which the simulations are done were in accordance with experimental steps and can be found below the structures in Figure S1 (Supporting Information).

Characterization of AuNPs and AuNP−MB Conjugates. The shape and size of the synthesized gold nanoparticles before and after their functionalization by MBs were visualized using transmission electron microscopy (TEM). As shown in Figure 1a, the spherical shape of the particles was confirmed. In Figure 1b, a clear difference can be observed in the thickness of the capping layer prior to and after the functionalization step (approximately 4−5 nm). This observation confirms the conjugation of the MBs onto the AuNP surface as reported before elsewhere.[45] The capping layer before the functionalizing step consists of citrate anions. Since the protocol used for attaching the MB described in the experimental section assures maximum DNA loading on AuNP surface, avoiding unwanted adsorption of MB onto AuNP surface,[46,47] this thickness difference can be attributed to the length of MBs in the closed form. Shapes and size distributions of the AuNPs after the functionalizing step did not change with respect to the nonfunctionalized ones.

Initial Studies. In order to investigate the accuracy of the theoretical predicted melting points, prior to synthesizing the three designed MBs (with thiol linker at 3′ ends and the three fluorophores at the 5′ ends),

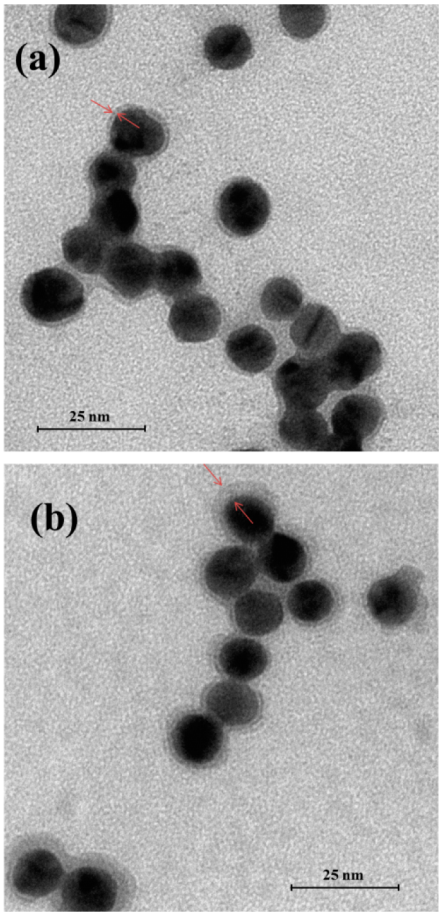

Figure 1. Transmission electron microscopy images of the AuNPs (a) prior to and (b) after functionalization with MBs. The red arrows highlight the thickness of the capping layer.

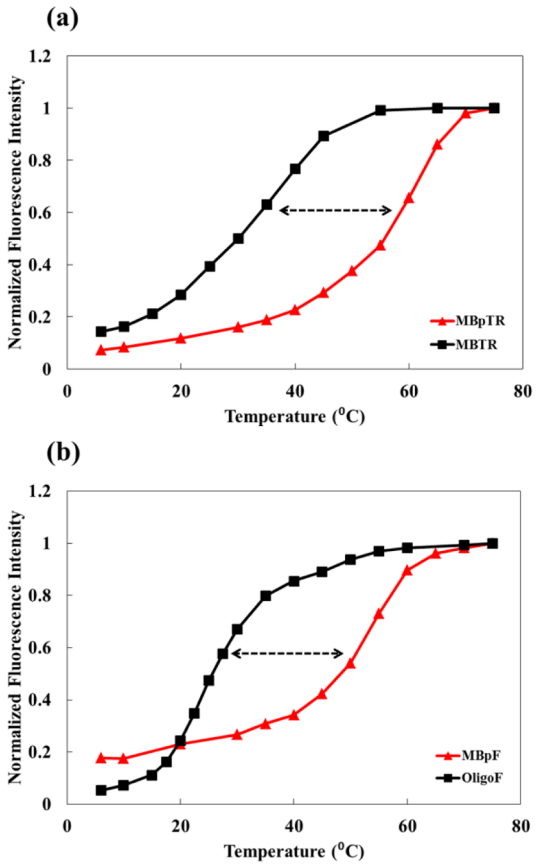

Figure 2. Comparison of melting curves obtained from the MBs with perfectly matched stems (red lines with triangle markers) with unusual less stable MBs (black lines with square markers): (a) MBpF and oligoF (b) MBpTR and MBTR. All experiments were carried out in PBS buffer (10 mM phosphate, 0.3 M NaCl, pH 7.4).

a few initial experiments were set up. Two MBs, one with the same sequence as oligoTR and the other with almost the same sequence but without any internal loops (with perfectly matched stem region), were synthesized in small quantities (MBTR and MBpTR in Table1). The 3′ ends of both MBs were modified with Dabcyl and the 5′ ends with the FAM. The aim was to study the agreement of the melting point of the theoretical predicted structure with that of oligoTR as one of the designed structures.

The melting curves of the synthesized structures can be observed in Figure 2a. The estimated T_m of the probes derived from the experimental melting curves, as well as their theoretical predicted T_m from the mfold tool can be observed in Table 2. The predicted T_m for MBTR and MBpTR structures were 37.8 and 62.6 °C, respectively. As is apparent from the results, the experimental T_m of the structures are in good accordance with the predicted values. The other important observation is that introducing the mismatch base pairs has a significant effect on destabilizing the MBs. In this example, inserting three mismatch base pairs in a rather stable MB (T_m = 62 °C) has considerably shifted the T_m to lower temperatures.

TABLE 2. Comparison of the Theoretically Predicted and Experimentally Obtained Melting Temperatures of the Designed MBs

probe	predicted T_m (°C)	experimental T_m (°C)
MBTR	37.8	35
MBpTR	62.6	60
OligoF	22.4	24
MBpF	59.9	55

To investigate the quenching ability of the AuNPs and their effect on the experimental T_m values of the attached MBs, in comparison to the theoretically predicted ones, another set of experiments was performed. Similar to the previous experiment, two MBs, one with the same sequence as oligoF and the other with perfectly matched stem region (MBpF), were ordered. The 3′ ends of both MBs were modified with a thiol linker, and their other ends were modified with FAM as the fluorescent label. After the MBs were loaded on AuNPs individually, their corresponding melting curves were recorded (Figure 2b). The obtained melting curves clearly approved the theoretically designed structure, as the distance between the

FAM and the AuNP surface in the closed and open forms satisfied the conditions mentioned in the experimental section. The values of the T_m obtained for both structures from the melting curves were also in agreement with the predicted ones (Table 2), implying that the thiol linker and the attachment procedure had no unwanted effect on the desired T_m temperatures. As is obvious from the melting curves, inserting two mismatch base pairs and an internal loop into a stable double helix, destabilized the MB to the desired degree.

AuNP–MB Nanothermometers. After initial experimental investigations, three final MBs (oligoF, oligoTR, and oligoA) were synthesized. There are several possible architectures for nanothermometers based on the MBs and AuNPs as the core of the design. The reason to select the 13 nm AuNPs was 2-fold, to have a carrier on which plenty of the same or different MBs could be anchored and also to take advantage of its strong surface plasmon resonance absorption, which makes it a rather global quencher for the fluorophores. The result of such assemblies is sensitive probes that have the flexibility to be adopted for specific conditions. In this section some possible designs are introduced and discussed.

Single MB Nanothermometers. On the basis of the desired temperature range, the simplest form of a nanothermometer can be made by conjugation of several same type MBs (oligoF or oligoTR or oligoA) with AuNPs. The aim of this part of the study, in addition to test MBs of different thermostability as sensing elements, was to investigate the ability of AuNPs as so-called universal quenchers of the fluorophores by which the MBs were labeled. The results of such study will be helpful to build more flexible temperature nanoprobes.

The schematic structures of single MB nanothermometers before and after their melting points are shown as insets of Figure 3. Before the melting point of each probe, the corresponding fluorophores of the same type are close to the AuNP surface and, because of two main mechanisms, the nanometal surface energy transfer (NSET) and fluorescence resonance energy transfer (FRET), are in quenched state. By increasing the temperature and opening the MB structures, the consequent increase in the distance between the fluorophores and the AuNP surface will turn on the nanoprobes.

Parts a–c of Figure 3 show the fluorescence spectra of oligoF, oligoTR, and oligoA recorded at various temperatures (6–60 °C). As can be seen, compared to the other two probes, oligoF is quenched more efficiently at the lowest temperatures. Indeed, such an observation was expected as the maximum emission wavelength of FAM is located within the surface plasmon resonance (SPR) band of the 13 nm AuNPs. The obvious fluorescence emission enhancement of all three probes upon temperature increase confirms the effectiveness of the AuNPs as good quenchers for all of the fluorophores. It seems that the efforts for designing the sequence of MBs, to satisfy their desired thermal stability (T_m) and length, was successful. The latter parameter was very critical because if the fluorophore could not be brought far enough from the AuNP surface, it might still be in the quenched state.

As stated previously, one of the complications in the current study was to design a long-stem MB by a melting point around 22 °C. Taking a look at the melting curve of oligoF at Figure 3d, it seems that the oligoF's melting point of 23 °C is good enough to satisfy these requirements. The melting curves of oligoTR and oligoA probes (Figure 3e,f), showing T_m of 40 and 50 °C, respectively, are also very close to those predicted in simulations. These curves are the result of sketching the variation in the maximum fluorescence emission of each MB (520 nm for oligoF, 670 nm for oligo TR, and 484 nm for oligoA) *versus* temperature. The melting curves shown in Figure 3 are normalized to the maximum fluorescence intensity of the probes. Each point of the melting curves is also the mean value obtained from three replicate experiments (by fabrication of the probes and recording their spectra at different temperatures).

A point that is worth noting is that the AuNPs was not observed to have any negative, temperature-dependent behavior on the MBs. To further confirm this, the melting behavior of each MB was investigated individually before attachment on AuNPs. The dashed curves shown in Figure 3 are the normalized melting curves of free MBs. As it is obvious from Figure 3, in comparison to the conjugated probes, no detectable melting behavior could be observed for free oligoTR and oligoA MBs. A very small improvement in the fluorescence signal of the free oligoF can be observed that could be attributed to the structural change of FAM in the closed and open forms, and also the increase in the emission of FAM itself at higher temperatures. It has been proven before that the behavior of the oligonucleotide attached FAM is nonlinearly temperature dependent.[48] FAM has a partial negative charge that can be strongly repelled by the negative charge of DNA backbone phosphates, particularly in the closed form, which result in a slightly less fluorescent structural conformation. The transition of the MB to the open form at increased temperatures will result in a different more fluorescent conformation. However, this observation is not really significant compared to the conjugated one.

The temperature resolution, which means the minimum temperature difference to be significantly discriminated by a temperature sensor, was also evaluated for the proposed nanoprobes. It can be calculated as the product of the inverse of the slope of intensity *versus* temperature and the standard deviation of the

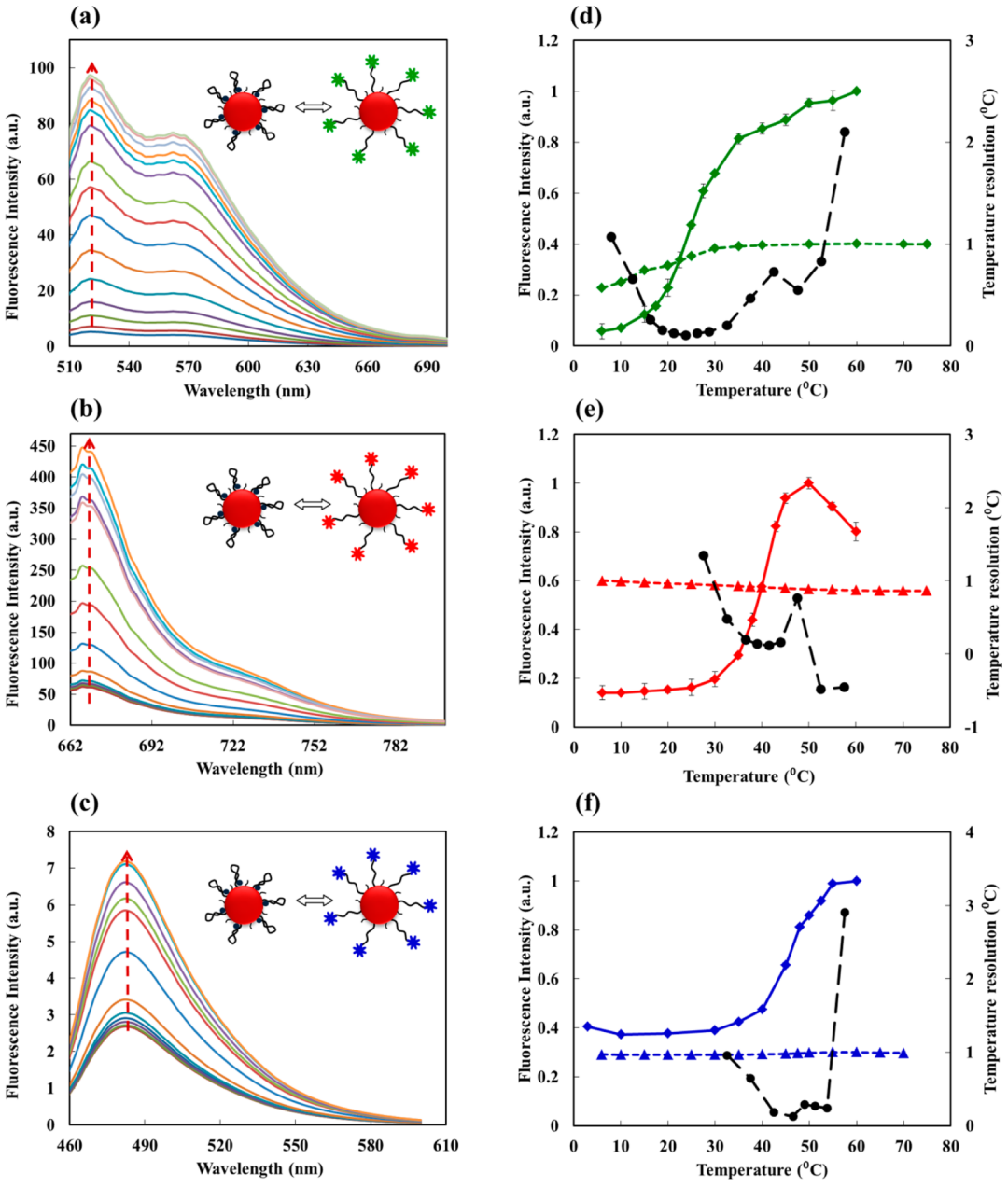

Figure 3. Fluorescence spectra of single MB nanothermometers based on (a) oligoF, (b) oligoTR, and (c) oligoA at different temperatures (6−60 °C). The inset schematics show the behavior of nanothermometers before and after melting of the attached MBs. Melting curves obtained from single MB nanothermometers (solid lines, rhombus markers) and also free MBs (dashed lines, triangle markers) are shown for (d) oligoF, (e) oligoTR, and (f) oligoA. The fluorescence intensities are normalized to their maximum intensities. The error bars of the melting curves represent standard deviation of three independent experiments. The temperature resolution of the single MB nanothermometers (black dashed lines, circle markers) is shown on the right axis of these subfigures. All experiments were carried out in PBS buffer (10 mM phosphate, 0.3 M NaCl, pH 7.4).

averaged fluorescence intensity.[9,15] In Figure 3d−f the temperature resolution curves (black plots with circle markers) by the right axis in each subplot can be seen for oligoF, oligoTR, and oligoA, respectively. Considering the dependence of the temperature resolution to the slope of the variation in the fluorescence signal, the best (lowest) resolution of each probe can be found around its melting point. The melting curve of oligoTR at high temperatures does not reach a plateau and decreases to some extent (Figure 3e), resulting in a negative slope. The reported negative temperature resolution is a result of this negative slope (−0.5 °C). Although this negative part of the melting curve can be used for thermometry, as stated in Table 3, the working range of this probe was set to 30−45 °C. Indeed, using oligoT as a helper strand significantly increased the stability and the repeatability of the nanothermometers (results not shown). Since the three designed MBs are appended with 10-T spacer at the 3′ end, which their lengths are the same as oligoT, the overall

TABLE 3. Melting Point, Temperature Resolution, and Working Range of the Synthesized Nanothermometers

sequence	T_m (°C)	temperature resolution (°C)	working range (°C)
nano probe (oligo F)	23	0.10—0.46	15—35
nano probe (oligo TR)	40	0.11—0.47	30—45
nano probe (oligo A)	50	0.12—0.24	40—55
two-MB probe	24, 41	0.06—0.47	15—46
multiplex probe	23, 41, 51	0.07—0.46	15—57

sterical effect maximizes the formation of the stem—loop structures near AuNP surface. The ratio of activated MBs and oligoT strands (2:1) was experimentally optimized to achieve the best performance of nanothermometers, where a balance between the repeatability of their melting curves and their signal intensity was observed. In addition to employment of the helper strand, some other affecting conditions including the type of buffer, reducing agent, salt concentration, heating, and sonication were also studied and optimized in functionalization step.

In the first three rows of Table 3, including melting points and temperature resolution, the working range of the studied three single MB nanothermometers can be found. It should be noted that the mentioned working ranges reported here only cover those temperatures for which the resolution is less than 0.5 °C. The working range of the probes can be extended upon a specific application for which high sensibility is not necessary. Comparing the temperature resolution plots of the three nanoprobes, oligoF covers a little more temperature range with satisfactory resolution. This can be attributed to the shape of the melting curves of the probes, as the melting of the oligoTR and oligoA happens at a narrower temperature range (about 5 °C compared to oligoF).

The agreement between the predicted melting points of the three single MB-based probes and their experimental values confirmed the designed structures. The AuNPs also performed well as good quenchers for all of the labels and as result can be used to load many different probes on their surface as both carriers and quenchers. By the proper selection of each of the proposed probes for the desired application, the temperature resolution of less than 0.50 °C can be obtained over a range of 15—60 °C, which to the best of our knowledge is better than resolution of the current fluorescent thermometers. In addition, the working range of the nanoprobes can be tuned by changing the sequence of the MBs for the desired T_m.

All above-mentioned experiments were carried out in PBS buffer (10 mM phosphate, 0.3 M NaCl, pH 7.4). It should be noted that the effect of Tris (pH 9.1) as a different buffer and also the PBS buffer with other pH values (7.8 and 8.0) were studied. Parts a—c of Figure 2S in the Supporting Information show that a change in the fluorescence intensity of the dyes in different

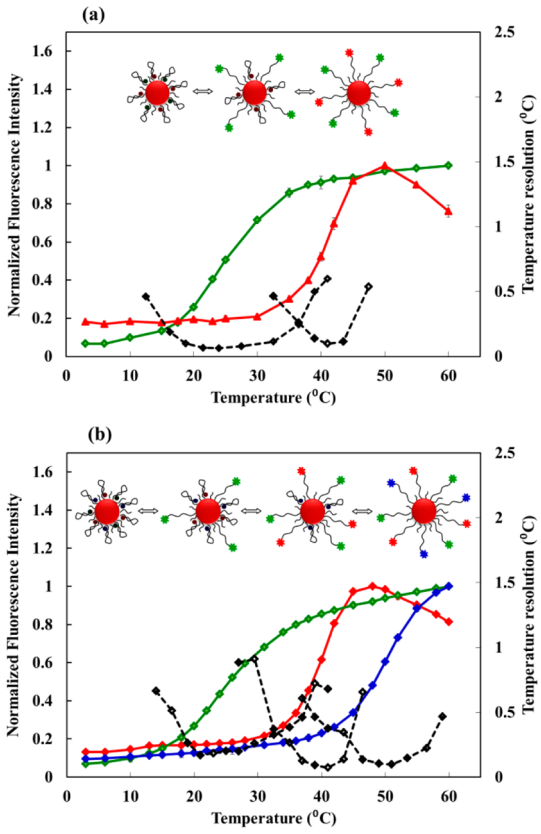

Figure 4. Melting curves of multiplex nanothermometers for (a) two-MB probe and (b) three-MB probe (left axis, solid lines) as well as the calculated temperature resolutions (black dash lines, right axis) in PBS buffer (10 mM phosphate, 0.3 M NaCl, pH 7.4). The inset figures schematically show the behavior of nanothermometers by increasing the temperature (3—60 °C). The fluorescence intensities were normalized to the related maximum fluorescence intensity.

buffer conditions happened, but the shape and position (melting point) of the melting curves were not affected. However, the normalized melting curves (Figure 2Sd—f in the Supporting Information) are not sensitive to the intensity related variations.

Multiplex Nanothermometers. To avoid using multiple probes for low-resolution temperature sensing covering a wide range of temperatures, it is possible to modify the surface of each AuNP with differently labeled MBs as sensing elements. Considering the extraordinary quenching ability of the AuNPs, such multiplex nanothermometers can be made by conjugating AuNPs with two or more tagged MBs. The size of the AuNPs (13 nm) provides enough free space to accept several same or different MBs. As examples of feasibility of such temperature-sensing nanoassemblies, two- and three-MB probes were synthesized and tested.

The two-MB probe was made by modifying the surface of the AuNPs by oligoF and oligoTR MBs. In Figure 4a, the response of the probe to the temperature is shown. Using the same excitation and emission wavelengths mentioned in a previous section, the normalized melting curves of the oligoF and oligoTR

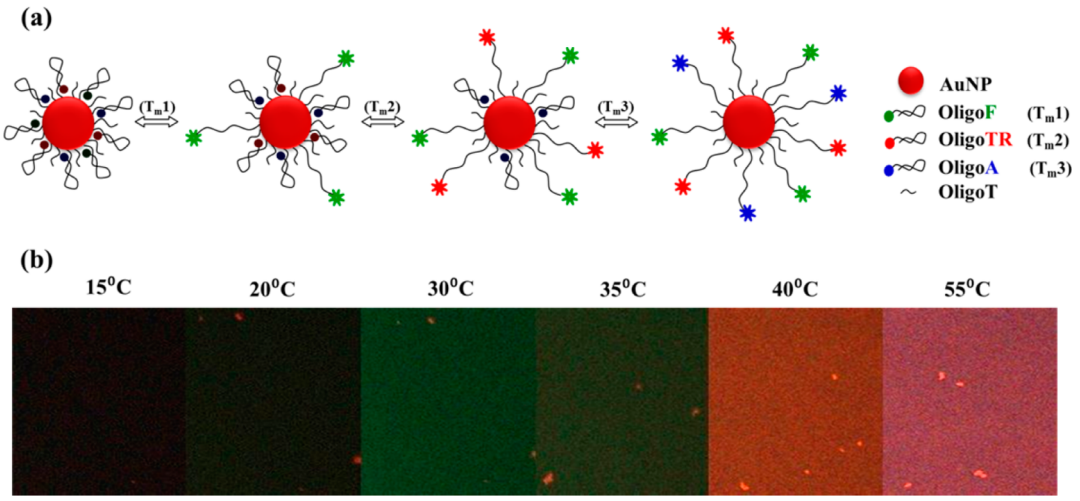

Figure 5. (a) Schematic presentation of the multiplex fluorescent nanothermometer. The oligoF modified with FAM (T_{m1} = 23 °C), oligoTR labeled with Texas red (T_{m2} = 38 °C), and oligoA tagged with Atto 425 (T_{m3} = 48 °C) are acting as the three RGB color channels for imaging purposes. (b) Confocal fluorescence microscopy images of a solution containing multiplex nanothermometer at different temperatures.

MBs were recorded. As can be seen, the shape and location of the melting curves are very similar to corresponding single-MB probes. The temperature resolution of the probe was also the same as single-MB probes. This observation confirmed that immobilizing two different types of MBs on the same AuNP, did not have a negative effect on their sensing functions.

Almost the same results were obtained with a three-MB probe composed of oligoF, oligoTR, and oligoA. To check the robustness of the latter probe, its response to temperature was recorded in three different days. The results in form of melting curves can be seen in Figure 4b and confirmed the good reproducibility of the nano probe. Such a probe can be used for sensitive and low resolution temperature sensing from less than 15 °C to temperatures higher than 60 °C for many applications at micro- and nanometer scale.

Thermal Imaging by Fluorescence Microscopy. One of the potential applications of the multiplex fluorescent nanothermometers is temperature imaging by fluorescence microscopy. To achieve this goal, a nanoprobe consisting of three MBs each tagged with different red-, green-, and blue-emitting fluorophores acting as three color channels immobilized on the AuNP surface can be used. To satisfy these conditions, we used oligoF as the green-emitting temperature-sensitive component, oligoTR as the red-emitting component, and oligoA as the blue-emitting one. Within a defined temperature range, the combination of these three emissions is expected to be unique under the fluorescence microscope for any given temperature. Such a colorful image would be helpful in biological imaging applications and also for temperature mapping in micro- and nanodevices.

In Figure 5a, the response of the proposed multiplex nanothermometer to the temperature is schematically illustrated from temperatures below the melting points of all three MBs where all of them are in the closed (quenched) form to a temperature higher than their melting points. In Figure 5b, the overlaid images obtained from a sample containing the synthesized probe at different increasing temperatures by excitation of fluorophores with corresponding specific lasers. The sample containing the probe was used without any preparation step. The fluorescence microscope was assisted with an incubator chamber with temperature control that allowed precise adjustment of the temperature. Additionally, the temperature of the cell solution was also controlled by a thermocouple probe immersed in the solution. Six images were taken by inverted laser scanning confocal microscope (Zeiss, LSM 780) equipped with a diode array detector. The diode array detector simultaneously records the emission from all three MBs, which results in full color images at different temperatures. As can be seen at 15 °C, all of the MBs are in quenched form and a dark image has been acquired. At 20 °C, the green emission from oligoF is more intense compared to the other MBs. The same can be concluded from the image obtained at 30 °C but as this point is after T_m of oligoF, the green emission is more intense. At this temperature the oligoTR has also started to glow but it is not very significant. At 35 °C the red and green emissions are comparable, but at 40 °C the red emission is dominant. Finally, at higher temperature (55 °C), the oligoA with blue emission is opened, which in combination with the emissions of the two other MBs gives rise to a new color.

CONCLUSIONS

In order to have multiplex nanothermometers based on MBs, it is important to use AuNPs which can act as global quenchers. In addition, the AuNPs should provide enough surface for the attachment of many MBs

and act as good scaffolds. On the basis of these requirements, it was found that the 13 nm AuNPs could be functionalized with one (single MB nanothermometer) or a combination of more than one type of MBs (Multiplex nanothermometers) to cover the desired temperature range. For future applications, based on the specific temperature range, the sequence of MBs can be designed accordingly. A temperature resolution of less than 0.50 °C was obtained over a range of 15−60 °C by the multiplex nanoprobe. The achieved low-temperature resolution, which indicates the high sensitivity of the probes, is a result of the increased slope of the melting curves. The efficient design of the unusual less stable MBs and the presence of AuNPs on which many MBs were attached, were two main reasons for this achievement. The reproducibility and precision of the probes were also successfully evaluated and confirmed. This is the first application of unusual MBs and AuNPs to construct the thermosensitive nanoassemblies.

The multiplex three MB nanoprobe in which MBs are tagged with red-, green-, and blue-emitting fluorophores acting as three color channels was successfully used for thermal imaging by fluorescence microscopy. This nanosensor can be used for thermometry and thermal imaging in microdevices. The ultimate goal of fabrication of these nanoprobes is the application of them in living cells which is under study in our group. An advantage of AuNP-based probes in biological applications, in addition to their biocompatibility, is that the surface of AuNPs can easily be functionalized to have target selective probes. To achieve maximum information content of obtained multivariate data sets and images, suitable chemometric techniques will also be employed.

METHODS

Materials. Sodium phosphate dibasic dihydrate, sodium phosphate monobasic monohydrate phosphate, sodium chloride, trisodium citrate dihydrate, dithiothreitol (DTT), tris-carboxyethylphosphine (TCEP), sodium dodecyl sulfate (SDS), and gold(III) chloride trihydrate were all obtained from Sigma-Aldrich. Concentrated hydrochloric acid and nitric acid were purchased from Merck (Darmsted, Germany). The oligonucleotides were synthesized by MWG Biotech (Germany) and used as received. The oligonucleotide stock solutions (100 μM) were prepared using a tris-EDTA buffer solution (10:1 mM, pH = 8.0) and stored at 4 °C. All buffer solutions were prepared in high-purity water obtained from a Milli-Q RG system.

Synthesis of AuNPs and Fabrication of Nanosensors. AuNPs with average diameter of 13 nm were synthesized *via* hot reduction of Au(III) ions to neutral gold atoms by sodium citrate solution.[49,50] Briefly, all glassware was cleaned in aqua regia (3 parts HCl, 1 part HNO_3) and rinsed with deionized water and then Millipore-filtered water. Two millilters of an aqueous solution of $HAuCl_4$ (50 mM) was poured into a two-neck reflux flask containing 98 mL of Millipore water with rapid stirring. Ten milliliters of a trisodium citrate solution (38.8 mM) was quickly added into boiling $HAuCl_4$ solution, which resulted in a change in the solution color from yellow to red. The solution was refluxed for an additional 20 min and allowed to cool to room temperature while stirring. The concentration of synthesized particles was determined by performing UV−vis spectroscopy measurements (their extinction coefficient of the 520 nm plasmon peak is about 2.4×10^8 L/(mol $\times$ cm). The color of synthesized AuNP colloid was burgundy red, and it was further characterized by dynamic light scattering (DLS) and transmission electron microscopy (TEM) techniques (Figure S5, Supporting Information). TEM images were captured on a FEI Tecnai G2 20 TWIN transmission electron microscope operating at 200 kV. The sample solution was single drop (10 μL) cast onto carbon-coated copper TEM grids and allowed to dry in air for several hours at room temperature. The DLS experiment was performed using a particle analyzer (Malvern Zetasizer Nano ZS). It should be noted that the synthesis of the gold nanoparticles was performed several times to obtain the more stable particles in the initial step. Finally, the approved AuNP solution was stored at 4 °C for all further experiments including assembling the single-MB and multiplex nanothermometers.

Immobilization of the AuNPs with activated thiol-modified MBs was performed in the presence of anionic surfactant (SDS), as it has been demonstrated to make the AuNP solution much more stable, even at high concentrations of Na^+.[46,47] First, the disulfide bond between the synthesized thiol modified MBs should be cleaved by addition of the freshly prepared TCEP in acetate buffer (pH 5.2) as a reduction agent. Resultant mixture was incubated at room temperature for 1h.Then, a solution containing a mixture of the freshly activated thiol modified MB and oligoT as the helper strand,[40] was added into 3000 μL of suspension of the AuNPs (13 nM) in 10 mM phosphate buffer (PB) containing SDS (0.01%, v/v) at pH 7.4. The final concentrations of the MB and the helper strand were 2 μM and 1 μM respectively. After 25 min incubation with gentle shaking, which allowed the self-assembly of MBs through the Au−S bond, the MB/AuNP mixture was exposed to the so-called aging step including a stepwise increase in the concentration of NaCl until a concentration of 1.0 M NaCl was reached. The concentration of NaCl was increased in 0.05 M steps, using a 2 M NaCl stock solution. The mixture was then sonicated for 10 s followed by 20 min incubation on the shaker at room temperature. The aging step was followed by incubation overnight at room temperature. To remove excess oligonucleotides, the mixture was centrifuged (18000 rpm, 20 min, 10 °C). The precipitate was washed three times with pure water, and finally dispersed in 1000 μL of measurement buffer (0.3 M NaCl, 10 mM PB, pH 7.4).

In order to confirm the attachment of the thiolated MBs onto AuNP surface *via* the covalent bond, in a comparison study, the functionalization protocol was carried out using both thiolated and nontiolated oligoF MBs. The color of nonthiolated oligoF-AuNP solution turned from red to blue by increasing the Na^+ concentration during the aging step while the thiolated oligoF-AuNP solution remained red until the end of aging step. The aggregation of insufficiently protected AuNPs is the reason for turning the red color of the solution to blue in higher ionic strengths. This observation emphasized the role of thiol bonds in functionalization of the AuNPs and confirmed the synthesis procedure.

To fabricate the multiplex nanoprobe the same procedure was used except that, a mixture of three activated MBs (with equal proportions) and the helper strand was added to the AuNP suspension. The final concentrations of each MB in this mixture were 2 μM and the concentration of the helper strand was 1 μM. The design of the three MBs was made in such a way that the length of their stem region and size of their loops are almost the same. This provides equal chance for them to win the competition of occupying the surface of AuNPs.

Fluorescence Measurements. All fluorescence measurements were performed by a Cary Eclipse fluorescence spectrophotometer. The three single probes, FAM, Texas Red, and Atto-425 were excited at 495, 585, and 440 nm, and the fluorescence emission spectra were collected from 510 to 700 nm, 600 to 800 nm, and 460 to 600 nm, respectively. A slit width of 10 nm

was used in both excitation and emission mode, while the photomultiplier tube voltage by the detector was set to 700 V. The temperature of the contents of the quartz cuvettes with 1 cm path length and maximum volume of 1 mL used in this study was adjusted with a thermostat controlled cell holder. Melting curves were obtained by plotting the fluorescence intensity at maximum emission wavelength *versus* temperature from 3 to 60 °C at a linear heating rate of 20 °C/h. Although kinetic studies demonstrated that a 5 min period was enough to reach an equilibrium state, where the maximum fluorescence intensity of probe was achieved, recording the fluorescence spectra was performed in 15 min increments.

Fluorescence microscopy images (Figure 5) were taken on an LSM 780 laser scanning confocal microscope (Zeiss) with a 20*x*/0.8 plan-apochromat objective. Lasers used for FAM, Texas Red, and Atto-425 were 405, 490, 555, and 595 nm, respectively.

Conflict of Interest: The authors declare no competing financial interest.

Supporting Information Available: Proposed structures of the three designed MBs assisted by mfold online tool and characterization of AuNPs by DLS and TEM methods; T melting curves of the nanothermometers at different pH and ionic strength conditions and temperature-cycled melting curves. This material is available free of charge *via* the Internet at http://pubs.acs.org.

Acknowledgment. We acknowledge the Danish Agency for Scientific Technology and Innovation (FTP Grant No. 274-08-0121) and the Institute for Advanced Studies in Basic Sciences (IASBS) for supporting this work.

REFERENCES AND NOTES

1. Zhang, C.; Xing, D. Miniaturized PCR Chips for Nucleic Acid Amplification and Analysis: Latest Advances and Future Trends. *Nucleic Acids Res.* **2007**, *35*, 4223–4237.
2. Dodge, A.; Turcatti, G.; Lawrence, I.; de Rooij, N. F.; Verpoorte, E. A Microfluidic Platform Using Molecular Beacon-Based Temperature Calibration for Thermal Dehybridization of Surface-Bound DNA. *Anal. Chem.* **2004**, *76*, 1778–1787.
3. Lowell, B. B.; Spiegelman, B. M. Towards a Molecular Understanding of Adaptive Thermogenesis. *Nature* **2000**, *404*, 652–660.
4. DeBerardinis, R. J.; Lum, J. J.; Hatzivassiliou, G.; Thompson, C. B. The Biology of Cancer: Metabolic Reprogramming Fuels Cell Growth and Proliferation. *Cell Metab.* **2008**, *7*, 11–20.
5. Ross, D.; Gaitan, M.; Locascio, L. E. Temperature Measurement in Microfluidic Systems Using a Temperature-Dependent Fluorescent Dye. *Anal. Chem.* **2001**, *73*, 4117–4123.
6. Shiraishi, Y.; Miyamoto, R.; Zhang, X.; Hirai, T. Rhodamine-Based Fluorescent Thermometer Exhibiting Selective Emission Enhancement at a Specific Temperature Range. *Org. Lett.* **2007**, *9*, 3921–3924.
7. Chen, Y. Y.; Wood, A. W. Application of a Temperature-Dependent Fluorescent Dye (Rhodamine B) to the Measurement of Radiofrequency Radiation-Induced Temperature Changes in Biological Samples. *Bioelectromagnetics* **2009**, *30*, 583–590.
8. Brites, C. D. S.; Lima, P. P.; Silva, N. J. O.; Millán, A.; Amaral, V. S.; Palacio, F.; Carlos, L. D. A Luminescent Molecular Thermometer for Long-Term Absolute Temperature Measurements at the Nanoscale. *Adv. Mater.* **2010**, *22*, 4499–4504.
9. Okabe, K.; Inada, N.; Gota, C.; Harada, Y.; Funatsu, T.; Uchiyama, S. Intracellular Temperature Mapping with a Fluorescent Polymeric Thermometer and Fluorescence Lifetime Imaging Microscopy. *Nat. Commun.* **2012**, *3*, 705–712.
10. Tsuji, T.; Yoshida, S.; Yoshida, A.; Uchiyama, S. Cationic Fluorescent Polymeric Thermometers with the Ability to Enter Yeast and Mammalian Cells for Practical Intracellular Temperature Measurements. *Anal. Chem.* **2013**, *85*, 9815–9823.
11. Kamp, H. D.; Higgins, D. E. A Protein Thermometer Controls Temperature-Dependent Transcription of Flagellar Motility Genes in Listeria Monocytogenes. *PLoS Pathogens* **2011**, *7*, e1002153.
12. Donner, J. S.; Thompson, S. A.; Kreuzer, M. P.; Baffou, G.; Quidant, R. Mapping Intracellular Temperature Using Green Fluorescent Protein. *Nano Lett.* **2012**, *12*, 2107–2111.
13. Li, S.; Zhang, K.; Yang, J. M.; Lin, L.; Yang, H. Single Quantum Dots as Local Temperature Markers. *Nano Lett.* **2007**, *7*, 3102–3105.
14. Yang, J. M.; Yang, H.; Lin, L. Quantum Dot Nano Thermometers Reveal Heterogeneous Local Thermogenesis in Living Cells. *ACS Nano* **2011**, *5*, 5067–5071.
15. Gota, C.; Okabe, K.; Funatsu, T.; Harada, Y.; Uchiyama, S. Hydrophilic Fluorescent Nanogel Thermometer for Intracellular Thermometry. *J. Am. Chem. Soc.* **2009**, *13*, 2766–2767.
16. Riedinger, A.; Guardia, P.; Curcio, A.; Garcia, M. A.; Cingolani, R.; Manna, L.; Pellegrino, T. Subnanometer Local Temperature Probing and Remotely Controlled Drug Release Based on Azo-Functionalized Iron Oxide Nanoparticles. *Nano Lett.* **2013**, *13*, 2399–2406.
17. Hamad-Schifferli, K.; Schwartz, J. J.; Santos, A. T.; Zhang, S. G.; Jacobson, J. M. Remote Electronic Control of DNA Hybridization Through Inductive Coupling to an Attached Metal Nanocrystal Antenna. *Nature* **2002**, *415*, 152–155.
18. Dias, J. T.; Moros, M.; del Pino, P.; Rivera, S.; Grazú, V.; de la Fuente, J. M. DNAas a Molecular Local Thermal Probe for the Analysis of Magnetic Hyperthermia. *Angew. Chem.* **2013**, *125*, 11740–11743.
19. Childs, P. R. N.; Greenwood, J. R.; Long, C. A. Review of Temperature Measurement. *Rev. Sci. Instrum.* **2000**, *71*, 2959–2978.
20. Roper, M. G.; Easley, C. J.; Legendre, L. A.; Humphrey, J. A.; Landers, J. P. Infrared Temperature Control System for a Completely Noncontact Polymerase Chain Reaction in Microfluidic Chips. *Anal. Chem.* **2007**, *79*, 1294–1300.
21. Fischer, L. H.; Harms, G. S.; Wolfbeis, O. S. Upconverting Nanoparticles for Nanoscale Termometry. *Angew. Chem., Int. Ed.* **2011**, *50*, 4546–4551.
22. Brites, C. D. S.; Lima, P. P.; Silva, N. J. O.; Millán, A.; Amaral, V. S.; Palacio, F.; Carlos, L. D. Thermometry at the Nanoscale. *Nanoscale* **2012**, *4*, 4799–4829.
23. Jaque, D.; Vetrone, F. Luminescence Nanothermometry. *Nanoscale* **2012**, *4*, 4301–4326.
24. McLaurin, E. J.; Bradshaw, L. R.; Gamelin, D. R. Dual-Emitting Nanoscale Temperature Sensors. *Chem. Mater.* **2013**, *25*, 1283–1292.
25. Tyagi, S.; Kramer, E. R. Molecular Beacons: Probes that Fluoresce upon Hybridization. *Nat. Biotechnol.* **1996**, *14*, 303–308.
26. Chen, C.; Wang, W.; Wang, Z.; Wei, F.; Zhao, X. S. Influence of Secondary Structure on Kinetics and Reaction Mechanism of DNA Hybridization. *Nucleic Acids Res.* **2007**, *35*, 2875–2884.
27. Owczarzy, R. Melting Temperatures of Nucleic Acids: Discrepancies in Analysis. *Biophys. Chem.* **2005**, *117*, 207–215.
28. Soto, A. M.; Kankia, B. I.; Dande, P.; Gold, B.; Marky, L. A. Incorporation of a Cationic Aminopropyl Chain in DNA Hairpins: Thermodynamics and Hydration. *Nucleic Acids Res.* **2001**, *29*, 3638–3645.
29. Brewood, G. P.; Rangineni, Y.; Fish, D. J.; Bhandiwad, A. S.; Evans, D. R.; Solanki, R.; Benight, A. S. Electrical Detection of the Temperature Induced Melting Transition of a DNA Hairpin Covalently Attached to Gold Interdigitated Microelectrodes. *Nucleic Acids Res.* **2008**, *36*, e98.
30. Barilero, T.; Le Saux, T.; Gosse, C.; Jullien, L. Fluorescent Thermometers for Dual-Emission-Wavelength Measurements: Molecular Engineering and Application to Thermal Imaging in a Microsystem. *Anal. Chem.* **2009**, *81*, 7988–8000.
31. Ke, G.; Wang, C.; Ge, Y.; Zheng, N.; Zhu, Z.; Yang, C. J. L-DNA Molecular Beacon: A Safe, Stable, and Accurate

Intracellular Nanothermometer for Temperature Sensing in Living Cells. *J. Am. Chem. Soc.* **2012**, *134*, 18908–18911.
32. Tyagi, S.; Bratu, D. P.; Kramer, F. R. Multicolor Molecular Beacons for Allele Discrimination. *Nat. Biotechnol.* **1998**, *16*, 49–53.
33. Dubertret, B.; Calame, M.; Libchaber, A. J. Single-Mismatch Detection Using Gold-Quenched Fluorescent Oligonucleotides. *Nat. Biotechnol.* **2001**, *19*, 365–370.
34. Das, P. C.; Puri, A. Energy Flow and Fluorescence Near a Small Metal Particle. *Phys. Rev. B* **2002**, *65*, 155416.
35. Dulkeith, E.; Morteani, A. C.; Niedereichholz, T.; Klar, T. A.; Feldmann, J.; Levi, S. A.; van Veggel, F. C.; Reinhoudt, D. N.; Müller, M.; Gittins, D. I. Fluorescence Quenching of Dye Molecules Near Gold Nanoparticles: Radiative and Nonradiative Effects. *Phys. Rev. Lett.* **2002**, *89*, 203002.
36. Fan, C.; Wang, S.; Hong, J. W.; Bazan, G. C.; Plaxco, K. W.; Heeger, A. J. Beyond Superquenching: Hyper-Efficient Energy Transfer from Conjugated Polymers to Gold Nanoparticles. *Proc. Natl. Acad. Sci. U.S.A.* **2003**, *100*, 6297–6301.
37. Dulkeith, E.; Ringler, M.; Klar, T. A.; Feldmann, J.; Munoz Javier, A.; Parak, W. J. Gold Nanoparticles Quench Fluorescence by Phase Induced Radiative Rate Suppression. *Nano Lett.* **2005**, *5*, 585–589.
38. Akhlaghi, Y.; Kompany-Zareh, M.; Hormozi-Nezhad, M. R. Multiway Investigation of Interaction between Fluorescence Labeled DNA Strands and Unmodified Gold Nanoparticles. *Anal. Chem.* **2012**, *84*, 6603–6610.
39. Russ Algar, W.; Massey, M.; Krull, U. J. The Application of Quantum Dots, Gold Nanoparticles and Molecular Switches to Optical Nucleic-Acid Diagnostics. *TrAC Trend. Anal.Chem.* **2009**, *28*, 292–306.
40. Song, S.; Liang, Z.; Zhang, J.; Wang, L.; Li, G.; Fan, C. Gold-Nanoparticle-Based Multicolor Nanobeacons for Sequence-Specific DNA Analysis. *Angew. Chem., Int. Ed.* **2009**, *48*, 8670–8674.
41. Zhang, J.; Wang, L.; Zhang, H.; Boey, F.; Song, S.; Fan, C. Aptamer-Based Multicolor Fluorescent Gold Nanoprobes for Multiplex Detection in Homogeneous Solution. *Small* **2010**, *6*, 201–204.
42. Huang, Y.; Zhao, S.; Liang, H.; Chen, Z. F.; Liu, Y. M. Multiplex Detection of Endonucleases by Using a Multicolor Gold Nanobeacon. *Chem.—Eur. J.* **2011**, *17*, 7313–7319.
43. Zuker, M. Mfold Web Server for Nucleic Acid Folding and Hybridization Prediction. *Nucleic Acids Res.* **2003**, *31*, 3406–3415.
44. Demers, L. M.; Mirkin, C. A.; Mucic, R. C.; Reynolds, R. A.; Letsinger, R. L.; Elghanian, R.; Viswanadham, G. A Fluorescence-Fased Method for Determining the Surface Coverage and Hybridization Efficiency of Thiol-Capped Oligonucleotides Bound to GoldT films and Nanoparticles. *Anal. Chem.* **2000**, *72*, 5535–5541.
45. Stakenborg, T.; Peeters, S.; Reekmans, G.; Laureyn, W.; Jans, H.; Borghs, G.; Imberechts, H. Increasing the Stability of DNA-Functionalized Gold Nanoparticles Using Mercaptoalkanes. *J. Nanopart. Res.* **2008**, *10*, 143–152.
46. Hurst, S. J.; Lytton-Jean, A. K.; Mirkin, C. A. Maximizing DNA Loading on a Range of Gold Nanoparticle Sizes. *Anal. Chem.* **2006**, *78*, 8313–8318.
47. Liu, J.; Lu, Y. Preparation of Aptamer-Linked Gold Nanoparticle Purple Aggregates for Colorimetric Sensing of Analytes. *Nat. Protoc.* **2006**, *1*, 246–252.
48. You, Y.; Tataurov, A. V.; Owczarzy, R. Measuring Thermodynamic Details of DNA Hybridization Using Fluorescence. *Biopolymers* **2011**, *95*, 472–486.
49. Grabar, K. C.; Freeman, R. G.; Hommer, M. B.; Natan, M. J. Preparation and Characterization of Au Colloid Monolayers. *Anal. Chem.* **1995**, *67*, 735–743.
50. Frens, G. Controlled Nucleation for the Regulation of the Particle Size in Monodisperse Gold Suspensions. *Nature* **1973**, *241*, 20–22.